UNIVERSITY *of York*

This is a repository copy of *Modelling the micro-structure of non-uniform conductive non-woven fabrics: Determination of sheet resistance*.

White Rose Research Online URL for this paper:
https://eprints.whiterose.ac.uk/89902/

Version: Accepted Version

White Rose
university consortium
Universities of Leeds, Sheffield & York

eprints@whiterose.ac.uk
https://eprints.whiterose.ac.uk/

Modelling the micro-structure of non-uniform conductive non-woven fabrics:

Determination of sheet resistance

A. N. Austin, J. F. Dawson, I. D. Flintoft and A. C. Marvin
Department of Electronics
University of York
York, UK
ana504@york.ac.uk, john.dawson@york.ac.uk, ian.flintoft@york.ac.uk, andy.marvin@york.ac.uk

Abstract—**The plane-wave shielding effectiveness of conductive non-woven fabrics is dominated by the sheet conductance over a wide range of frequencies until the effects of skin depth, and apertures start to influence the performance (typically at 1-10 GHz depending on the areal density). This paper describes models for determining the sheet conductance from knowledge of the type, quantity, orientation and contact resistance of the fibres in the fabricated material. The stochastic nature of these materials, their complexity and local scale variability has been included in the models and correlates well with experimental results. The anisotropic sheet conductance is modelled to within 1% of the measured value in the high shielding orientation and to within 2% in the orthogonal orientation using an inter-fibre contact resistance estimated to be 10 kΩ.**

Keywords: sheet resistance; shielding effectiveness; stochastic material; anisotropic material; circuit model; contact resistance

I. INTRODUCTION

Advanced non-woven materials are used throughout the aerospace, defence and medical industries, usually to provide lightweight, functional enhancement to existing composite structures which otherwise underperform. Applications include shielding for electromagnetic compatability, collapsible antenna reflectors and defibrillator electrodes.

The ability to optimise non-woven fabrics toward the diverse applications in which they exist necessitates accurate models of their structure. Once validated, these models can be applied to any number of application specific problems including thermal, structural and electromagnetic shielding.

This paper presents micro-structure models of non-woven fabrics and their translation to equivalent circuit models to allow the sheet conductance and hence shielding effectiveness to be predicted. The modelled sheet conductance is then compared with experimental measurement.

II. MATERIALS

A non-woven fabric is an array of discontinuous fibres that are formed into a sheet using a wet-laid process like that used for paper manufacture. Non-woven materials possess a complicated structure with varying local parameters such as thickness, areal density, and fibre angle. Fig. 1 shows a scanning electron microscope (SEM) image of a non-woven fabric, constructed from 12 mm long polyacrylonitrile carbon fibres (see Table I), stabilised using a polyester binder (5% by weight) along with a CAD model produced by the methods described below.
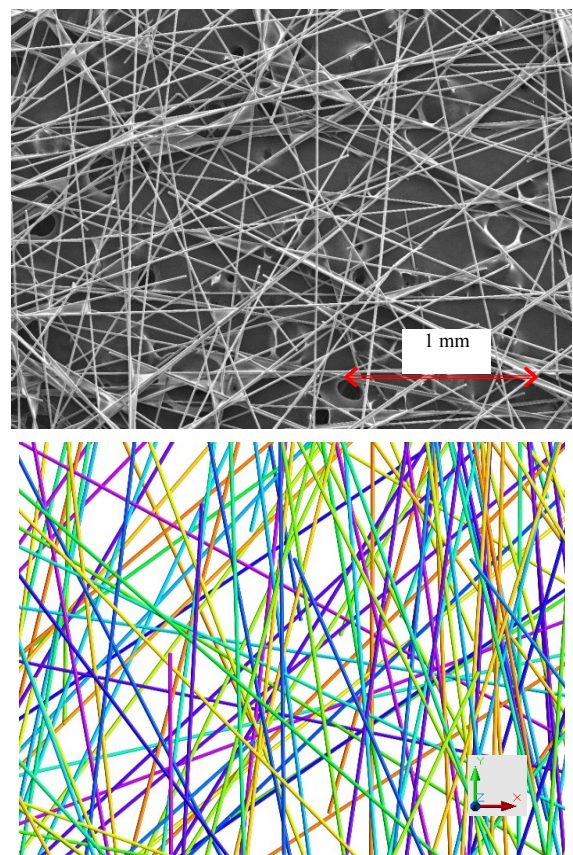

Fig. 1.   An SEM image of a non-woven material constructed of carbon fibre elements (top) and a 3D CAD model at a similar scale (bottom).

TABLE I.   PROPERTIES OF TOHO TENAX HTC 124 CARBON FIBRES.

Mass Density	Diameter	Electrical Conductivity	Length
ρ_f	d_f	σ_f	L_f
1820 kg m^{-3}	7 μm	72.6 kS/m	12 mm

Due to the local non-uniformity of the material, it is important to construct models which incorporate similar stochastic behaviour, as well as capturing the geometry and material properties, so that the statistical variability of results and effects of the sample size can be understood.

As the fibre length is small (millimetres) relative to the typical size in which these structures can be formed (meters), current must flow from one fibre to the next via contact points (junctions). The sheet conductance is anisotropic and is dependent upon the areal density, ρ_A, orientation of the fibres, φ, material thickness, t, the fibre resistance, R_f, and the inter-fibre contact resistance (R_j).

Fig. 2 shows shielding effectiveness measurements (see [1] and [2]) for non-woven carbon-fibre veils of various areal densities along with curves fitted to the Schelkunoff plane-wave shielding model [3]. The 0° orientation corresponds to the direction in which the veil is pulled from the wet-lay process during manufacture, and has the highest conductivity and hence the highest shielding effectiveness of the two orientations measured for each areal density. At low frequencies, when the skin depth is much greater than the sheet thickness, the shielding effectiveness of an equivalent homogeneous material of conductivity σ_{eff} is

$$SE = \tfrac{1}{2}\eta_0 G_s, \qquad (1)$$

where η_0 is the impedance of free-space and the sheet conductance is $G_s = \sigma_{eff} t$.
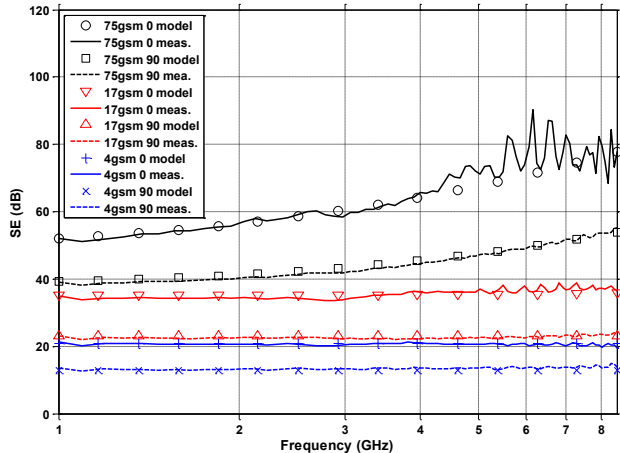

Fig. 2.   Measured shielding effectiveness data and Shelkunoff plane wave model for various areal densities showing that the flat, conductance dominated region extends beyond 1 GHz for a range of areal densities. The difference in shielding at 0° and 90° orientations can also be seen.

In order to predict the shielding performance of non-woven materials we therefore need to determine the sheet conductance from knowledge of the fabrication parameters.

If we assume the contact resistance between fibres is negligible ($R_j = 0$) then well above the percolation threshold the sheet conductance of the veil takes the form

$$G_s = \sigma_f \frac{\rho_A}{\rho_f} \Phi(\varphi), \qquad (2)$$

where $\Phi(\varphi)$ is a geometrical factor which depends on the arrangement of the fibres and the angle of current flow, φ. For example, in a structure in which all the fibres are aligned with the $\varphi = 0^\circ$ direction (parallel but not in contact with each other) $\Phi(0^o) = 1$ and $\Phi(90^o) = 0$, whereas if the fibres were arranged like a square mesh with half the fibres at $\varphi = 0^\circ$ and half at $\varphi = 90^\circ$ then $\Phi(0^o) = \Phi(90^o) = 1/2$ since half the fibres would be available to conduct in each direction. For stochastic structures $\Phi(\varphi)$ is an average over the fibre angle distribution.

III.   MEASUREMENT METHODOLOGY

A.   Sheet conductance measurement

A two-electrode resistance measurement (Fig. 3 left) was used to determine the sheet conductance of six samples. The contact resistance between the electrodes and sample was previously determined and subtracted from the final results using the two-terminal resistor method described in [4]. The measurement uses electrode blocks which are positioned on top of the sample and secured with a 1 kg weight to ensure consistent contact. The electrodes (Fig. 3 right) are constructed from 10 cm long brass strips, separated by a distance of 10 cm, bonded to an insulating polymer block.

The measurements are carried out for two sample orientations, 0° and 90°, to determine the degree of anisotropy present in the samples. The non-woven structures considered here yield their highest sheet conductance in the 0° orientation due to the nature of the manufacturing process.

Fig. 3.   The sheet conductance test setup (left) and the measurement electrodes (right).

B.   Sample thickness measurement

The material thickness was determined using a digital micrometer which measures the average thickness over a 10 cm^2 area. The lowest measurement pressure setting (50 kPa) was used to avoid compressing the samples.

C.   Determining the fibre angle distribution

The degree of fibre alignment is influenced by the mechanical processing conditions. In order to determine the fibre angle distribution of a particular sample, a Hough Transform optical extraction technique was used [6]. This technique allows straight lines (fibres) to be detected in an SEM image of the

veil allowing the number and angle of fibres to be calculated. Averaging this process over a number of images provides data from which an accurate probability density function (PDF) can be derived. Fig. 4 illustrates the detection of fibres by the Hough Transform in a typical non-woven sample.
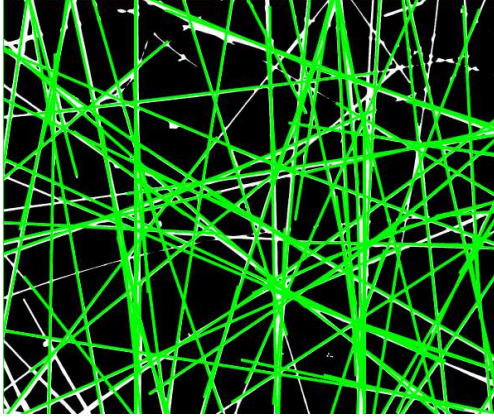

Fig. 4. The Hough Transform technique allows fibres to be counted and their angles to be calculated from SEM images of the structure: Here green lines are detected fibres while white lines show undetected fibres.
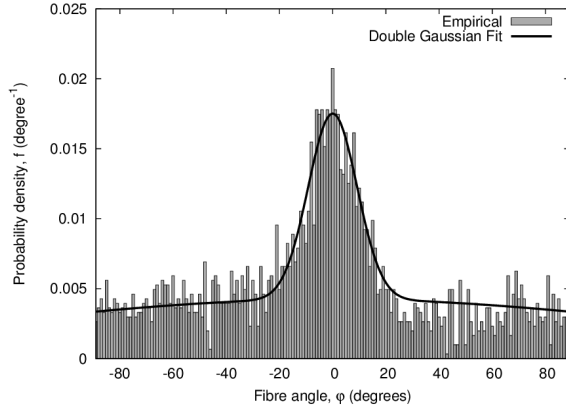

Fig. 5. The fibre angle distribution for a 4 g/m^2 density non-woven fabric.

A double Gaussian probability density function,

$$f(\varphi) = a_1 e^{-((\varphi-b_1)/c_1)^2} + a_2 e^{-((\varphi-b_2)/c_2)^2}, \qquad (3)$$

was found to provide a good fit to the data (with φ in degrees), as shown in Fig. 5. The fitted coefficients are: $a_1 = 1.313\times10^{-2}$, $b_1 = 0.0$, $c_1 = 12.98$, $a_2 = 4.186\times10^{-3}$, $b_2 = 0.0$ and $c_2 = 184.6$. Other studies have indicated that this distribution may vary from Gaussian to Lorentzian depending on the manufacturing process [5].

IV. Modelling methodology

In order to understand the properties of the non-woven veils we have developed a means of creating CAD models of a veil which is useful for numerical electromagnetic modelling and the development of circuit models for sheet conductance determination, as described later in this paper.

A. Micro-structure generation

An algorithm was written to generate a 3D model of the non-woven fabric, incorporating factors such as the fibre density, diameter, length, target areal density, thickness and fibre angle distribution. As some of these factors vary locally across the veil, it was important to understand the effects of region size on the degree of variability in the sheet conductance, particularly when comparing measurement and simulation results. Hence we generated a model of a large veil from which a number of smaller samples can be taken analogously to the experimental process. The coordinate system used to define the veil is shown in Fig. 6 and a typical veil with four sample areas is shown in Fig. 7.

The algorithm for generating the model was implemented using the MATLAB[7]/Octave[8] programming language and consists of the following steps:

1. Define a volume larger than the veil size (in directions x and y) by at least half a fibre length and equal to the thickness (in the z direction). The area is made larger than the veil size (shown as the blue rectangle in Fig. 7) so that partial fibres are produced that intrude into the volume at the edges, as they would for any veil cut from a larger piece.

2. Randomly generate the desired number of sample regions (shown red in Fig. 7).

3. Generate a fibre midpoint within the volume using a uniform random distribution in x, y and z.

4. Generate the azimuthal angle (φ) for the fibre according to the empirical angular PDF of Fig. 5.

5. Generate the elevation angle (θ) with a uniform distribution, but limiting its range so that the end-points of the fibre are within the thickness of the veil.

6. Determine mass of the fibre that lies within veil and add this to a mass accumulator.

7. Determine if the fibre is within each sample region. If inside, truncated fibre at the edge of the sample and add the segment end-points to a separate list for each sample region.

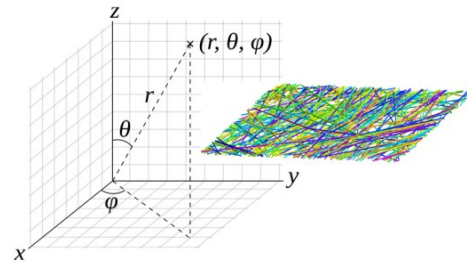8. Repeat 3-7 until the mass of veil gives required areal density.

Fig. 6. The co-ordinate system used to generate the veil model. z is in the direction of the sample thickness, x is along the 0° orientation and y along the 90° orientation.

The generated veil samples can then be post-processed to create CAD models for numerical simulation or used to generate a resistor network model to determine the conductance of the sample. Note that this is a "soft-core" model in which overlapping fibres pass through each other.

Statistical information is produced by the veil generation algorithm and includes: the number of active fibres, the average segment length, the sample areal density, the number

of segments, the average number of connections per fibre and the void volume fraction (VVF).

It is important to note that these 3D stochastic fibre models are different to those usually constructed in 2D percolation analysis [9]. This is because the sample thickness in these models varies with the areal density and so the statistics governing the inter-fibre connections will be different.
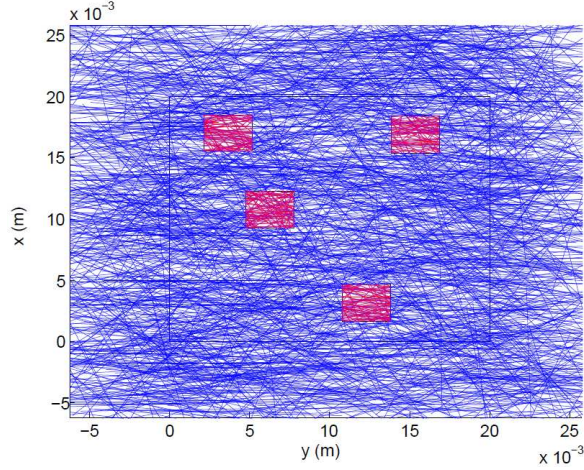

Fig. 7.   A plan view of the stochastic fibre model veil region, directly generated by the algorithm within MATLAB. Four samples (red) are shown here – typically 32 samples were used to generate the data in this paper.

B.   Resistor network model

A resistor network for each sample is formed by identifying all of the contact points by searching for fibre pairs which lie within a defined separation distance (see Fig. 8). Fibres whose minimum separation distance is less than one fibre diameter (7µm) are regarded as contacting at the points of closest approach. Care must be taken in the "corner cases" of parallel and collinear fibres. It is also necessary to identify the points of contact between the fibres and the boundaries of the sample across which the voltage is applied for the polarization under consideration. Further statistical information is extracted during this phase, such as the distribution of segment lengths between contact points and the number of contacts.

The list of contact points is then used to construct a circuit net-list for the fibres in the sample for subsequent modified nodal analysis using a SPICE circuit simulator [10]. During the construction of the net-list the ends of each fibre are connected to the reference node through a $R_\infty = 100\,\text{M}\Omega$ resistor to eliminate the need for an iterative pruning of floating parts of the structure that would otherwise lead to a singular modified nodal analysis matrix. A DC source is applied between the nodes corresponding to two opposite boundaries of the sample and the current through the source is monitored to allow the conductance of the sample to be determined. A number of simple validation cases similar to the one in Fig. 8 were generated to test the net-list generation algorithm for the various ways in which fibres may form contacts.

V. RESULTS

A.   Measured sheet conductance

The measured sheet conductance is shown in Fig. 9. It increases with the areal density of the veil due to the increasing number of conductive pathways that exist in the

structure. The anisotropy due to fibre angle distribution can be clearly seen in the difference between the 0° and 90° orientation conductance measurements.
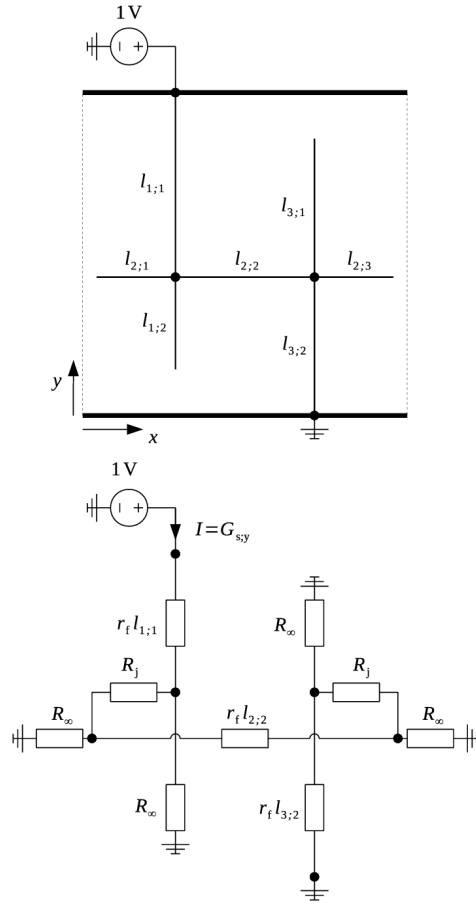

Fig. 8.   A simple collection of fibres (top) and the corresponding resistor network (bottom). Here $l_{i;j}$ is the length of the j-th segment of the i-th fibre and $r_f = 2/(\pi\sigma_f d_f^2)$ is the fibre resistance per unit length.
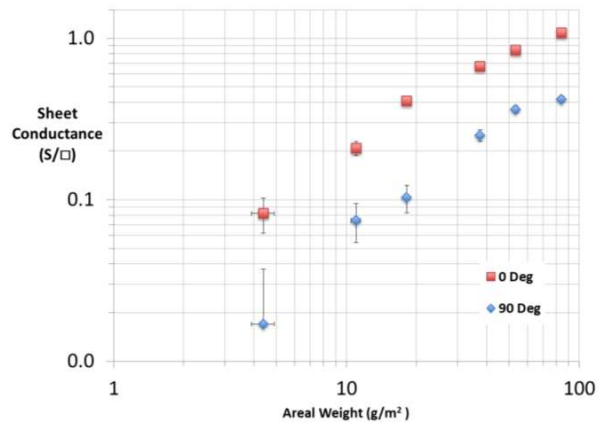

Fig. 9.   The measured sheet conductance of non-woven fabrics of various areal densities. Results for 0° and 90° orientations are shown.

B.   Material thickness and inter-fibre contacts

The measured thicknesses of various areal densities of non-woven veils are shown in Fig. 10. The thickness is seen to increase linearly with areal density, due to the manufacturing process used. This allows the thickness for the modelled veils

to be set to realistic values and extrapolated for the lighter densities which are not available as production samples. This also affects the number of contact points: Many percolation studies have shown that in 2D structures the number of contacts is proportional to square of the areal density as the density increases [12]. Due to the high aspect-ratio of the fibres (approaching 2000:1) and small sample thickness we expected similar behaviour in the 3D veil models reported here.
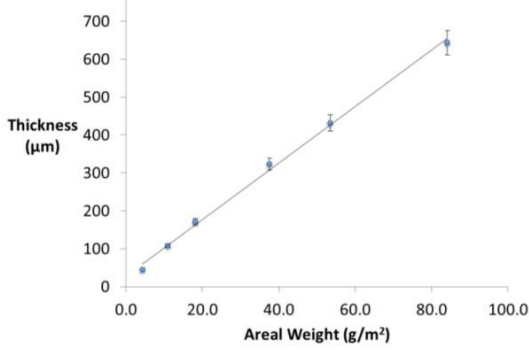

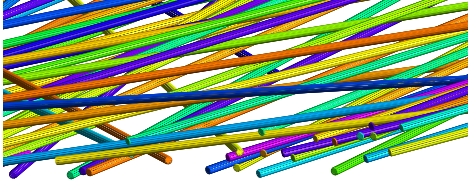Fig. 10. The measured relationship between average sample thickness and areal density.

Fig. 11. A cross-section of the modelled structure, exported to a 3D CAD format, showing the cylindrical meshing of the fibres.

C. CAD output

The fibres generated can be meshed as cylinders, as shown in Fig. 11, using a tool such as GMSH [13]. The meshed structure can then be imported into simulation tools for full-wave electromagnetic analysis of the broadband behaviour.

D. Variation of sheet conductance with areal density

The simulated sheet conductance is shown in Fig. 12 and Fig. 13 for the 0° and 90° orientations respectively. The sheet conductance for the 0° orientation, G_s^0, has an asymptotic behaviour with $\Phi \sim 0.75$, which is somewhat higher than that of a regular square mesh. The percolation threshold occurs at very low densities for this orientation due to the high aspect ratio fibres. There is significant variability across the veil at low areal densities (<1 g/m^2), as shown by the variance in sample density and conductance. The sheet conductance for the 90° orientation, G_s^{90}, reaches a percolation threshold at high areal densities of around 0.5 g/m^2 and has a much lower $\Phi \sim 0.19$. This orientation also exhibits much greater variability across the structure compared to the $0°$ direction.

The effect of sample size on the modelled sheet conductance is shown in Fig. 14 and Fig. 15 for a range of areal densities. This aids our understanding about how small samples sizes can become before the results are compromised by high variability or other factors such as the percolation threshold. Smaller simulated sample sizes are preferable as they can be computed in run times of minutes rather than days. For the 0° orientation, the effect of the sample size reduces quickly as it
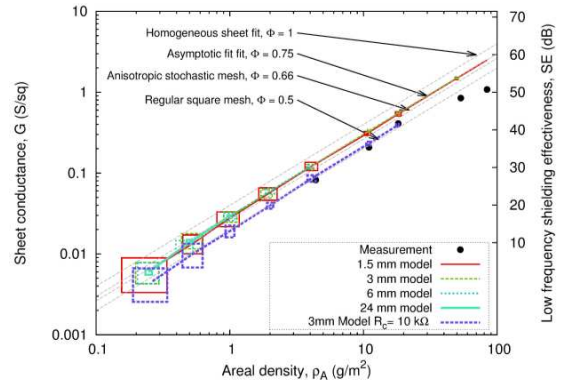

Fig. 12. Mean conductance G_s^0 versus areal density, with an inter-fibre contact resistance of $R_j = 0$. The error boxes show the one standard deviation model variation over 32 samples.

Fig. 13. Mean conductance G_s^{90} versus areal density with an inter-fibre contact resistance of $R_j = 0$. The error boxes show the one standard deviation model variation over 32 samples.
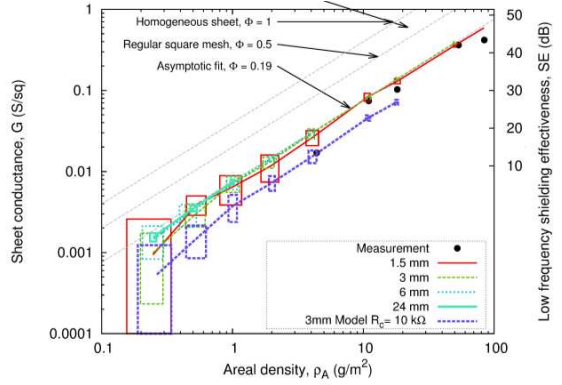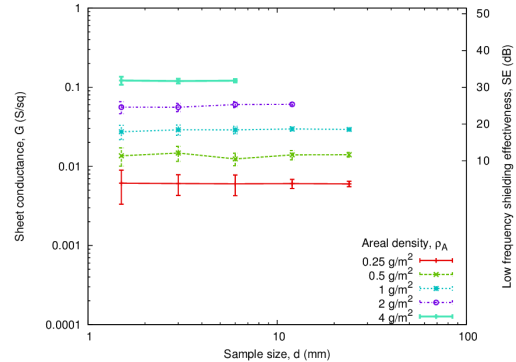

Fig. 14. Mean conductance G_s^0 with one standard deviation error bars versus sample size for multiple areal densities with zero inter-fibre contact resistance.
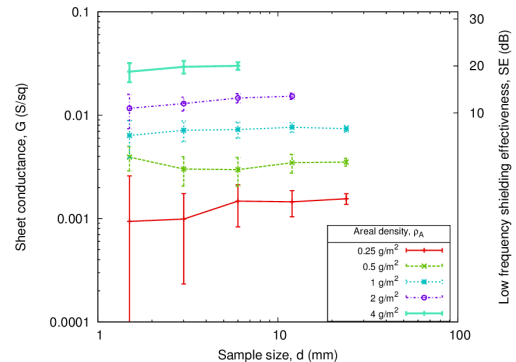

Fig. 15. Mean conductance G_s^{90} with one standard deviation error bars versus sample size for multiple areal densities with zero inter-fibre contact resistance.
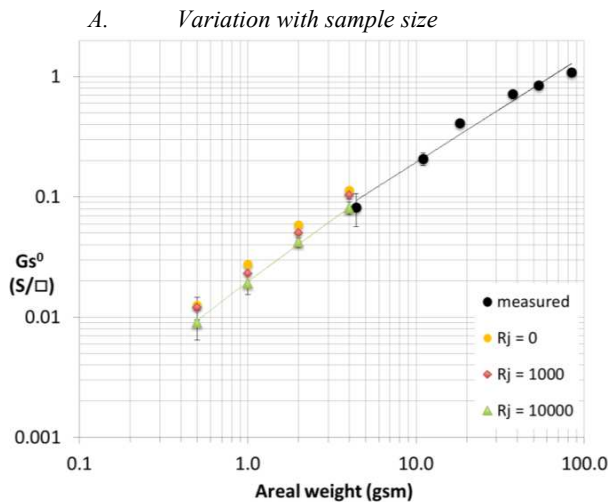
A. Variation with sample size

Fig. 16. Effect of different inter-fibre contact resistances (R_j) on the overall sheet conductance for the 0° orientation.
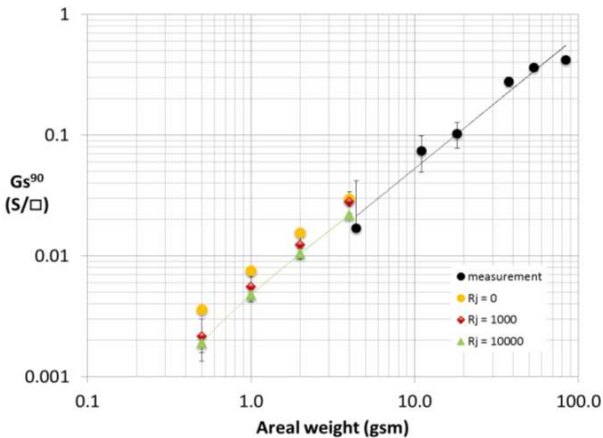

Fig. 17. Effect of different inter-fibre contact resistances (R_j) on the overall sheet conductance for the 90° orientation.

increases - typically samples of size 3 mm square or greater provide a low variability result.

For the 90° orientation at areal densities above $1g/m^2$ a sample size of 3 mm square remains large enough to allow an accurate simulation. However, the lighter (fictional) areal densities of 0.25 g/m^2 and 0.5 g/m^2 fail to percolate for sample sizes below 12 mm and a sample size greater than 24 mm is required to reduce the variability to a satisfactory level.

E. Estimated inter-fibre contact resistance

By increasing the inter-fibre contact resistance in the resistor model and comparing the asymptotic behaviour of the conductance to the measured data the contact resistance can be estimated. Fig. 16 and Fig. 17 show that a value of $R_j = 10k\Omega$ gives a good correlation between the modelled and measured sheet conductance results. This value of R_j is a similar order of magnitude to other reported contact resistances in stochastic fibre based materials where R_j is given as about 10 kΩ [14].

VI. CONCLUSIONS AND FURTHER WORK

A model of the microstructure for a class of non-woven fabrics has been presented which accurately predicts (within 1-2%) the anisotropic sheet conductance with realistic values for the inter-fibre contact resistance. This allows the low

frequency shielding effectiveness to be predicted. The statistical variation of the sheet conductance with sample size has been investigated and it has been shown that a minimum sample size exists below which it is difficult to get results representative of a larger sheet due to the stochastic variability of the properties.

For the ongoing full-wave computational work at higher frequencies (1-18 GHz) it is important that the microstructure is represented accurately and the work here gives some insight into the material behaviour with different sample sizes. In this frequency range skin-depth, aperture coupling, and porpoising effects, where current is carried through the thickness of the material with fibres that pass through it, may occur.

Work to measure the inter-fibre contact resistance is also underway using a 4-wire jig where the relative fibre angle and pressure can be varied.

REFERENCES

[1] A. N. Austin, J. F. Dawson, I. D. Flintoft and A. C. Marvin, "Analysis of the shielding properties of metalised nonwoven materials", *Electromagnetic Compatibility (EMC EUROPE), 2013 International Symposium on*, Bruges, 2-6 Sept. 2013, pp.526-531.

[2] A. C. Marvin, L. Dawson, I. D. Flintoft and J. F. Dawson, "A method for the measurement of shielding effectiveness of planar samples requiring no sample edge preparation or contact", *IEEE Transactions on Electromagnetic Compatibility*, vol. 51, pp. 255-262, 2009.

[3] S. A. Schelkunoff, "The Impedance Concept and Its Application to Problems of Reflection, Refraction, Shielding and Power Absorption", *Bell System Technical Journal,* Bell Systems, vol. 17, pp. 17-48, 1938.

[4] S. S. Cohen, "Contact resistance and methods for its determination", *Thin Solid Films,* vol. 104, pp. 361-379, 1983.

[5] F. Du, "Effect of nanotube alignment on percolation conductivity in carbon nanotube/polymer composites", *Physical Review B*, vol. 72, 121404, 2005.

[6] R. O. Duda and P. E. Hart, "Use of the Hough transformation to detect lines and curves in pictures", *Commun. ACM*, vol. 15, pp. 11–15, 1972.

[7] "MATLAB the language of technical computing", *The MathWorks, Inc.,* Natick, Massachusetts, US. http://uk.mathworks.com/products/matlab/, Accessed 29 January 2015.

[8] J. W. Eaton and J. B. Rawlings, "Ten Years of Octave — Recent Developments and Plans for the Future," in *Proceedings of the 3rd International Workshop on Distributed Statistical Computing (DSC 2003)*, pp. 1–12, 2003.

[9] I. Balberg, "Percolation thresholds in the three-dimensional sticks system", *Physical Review Letters,* vol. 52, pp. 1465-1468, 1984.

[10] L. W. Nagel and D. Pederson, "SPICE (Simulation Program with Integrated Circuit Emphasis)", EECS Department, University of California, Berkeley , no. UCB/ERL M382, April 1973. Available from: http://www.eecs.berkeley.edu/Pubs/TechRpts/1973/22871.html

[11] M. Žeželj and I. Stanković, "From percolating to dense random stick networks: Conductivity model investigation", *Phys. Rev. B*, American Physical Society, vol. 86, 134202 , 2012.

[12] W. Bao, "Modeling electrical conductivities of nanocomposites with aligned carbon nanotubes" *Nanotechnology,* vol. 22, 485704, 2011.

[13] C. Geuzaine and J.-F. Remacle, "Gmsh: a three dimensional finite element mesh generator with built-in pre- and post-processing facilities", *International Journal for Numerical Methods in Engineering,* vol. 79, no. 11, pp. 1309-1331, 2009.

[14] R. Mutiso, "Integrating simulations and experiments to predict sheet resistance and optical transmittance in nanowire films for transparent conductors", *ACS Nano,* vol. 7-9, pp. 7654-7663, 2013.